Journal of Solid State Chemistry 270 (2019) 205–211

Contents lists available at ScienceDirect

Journal of Solid State Chemistry

journal homepage: www.elsevier.com/locate/jssc

Magnetic properties of GdBB'Ge$_4$O$_{12}$; BB' = FeZn or GdCa

Diming Xu[a], Peter D. Battle[a,*], D.H. Ryan[b]

[a] Inorganic Chemistry Laboratory, Oxford University, South Parks Road, Oxford OX1 3QR, UK
[b] Physics Department and Centre for the Physics of Materials, McGill University, 3600 University Street, Montreal, Quebec, Canada H3A 2T8

ARTICLE INFO

Keywords:
Antiferromagnetism
Germanates
Gd Mössbauer spectroscopy
Fe Mössbauer spectroscopy
Neutron diffraction

ABSTRACT

Polycrystalline samples of $Gd_2CaGe_4O_{12}$ and $GdFeZnGe_4O_{12}$ have been synthesised via a ceramic route. Both were characterised by X-ray diffraction, magnetometry and Mössbauer spectroscopy; $GdFeZnGe_4O_{12}$ was also studied by neutron diffraction. They adopt the $SrNa_2P_4O_{12}$ structure: space group $P4/nbm$ with a = 10.0766(1), c = 5.1043(1) Å for $Gd_2CaGe_4O_{12}$; a = 9.7298(1), c = 4.7515(1) Å for $GdFeZnGe_4O_{12}$ at 293 K. $Gd_2CaGe_4O_{12}$ is paramagnetic for $2 \le T/K \le 300$ whereas $GdFeZnGe_4O_{12}$ is antiferromagnetic below 13.8(2) K. The six-coordinate Fe^{3+} and Zn^{2+} cations are disordered over the pseudo-cubic 4f sublattice and the Gd^{3+} cations occupy the eight-coordinate 2b sites. The Fe^{3+} and Gd^{3+} cations adopt an A-type, $\mathbf{k}$ = [0,0,½] antiferromagnetic arrangement with their ordered moments aligning in the xy plane. The Fe/Zn disorder results in relatively low ordered cation moments (Gd^{3+} = 6.02(13), Fe^{3+} = 3.84(15) μ_B) in the antiferromagnetic phase.

1. Introduction

Leonidov et al. have previously described [1] the luminescent properties of mixed-metal germanates which have the general formula $ABB'Ge_4O_{12}$, for example $Y_2CaGe_4O_{12}$. These materials adopt the tetragonal space group $P4/nbm$ (No. 125) and are isostructural with $SrNa_2P_4O_{12}$ [2]. Their structure thus consists of (001) sheets of $[Ge_4O_{12}]^{8-}$ groups, each group being comprised of four corner-sharing GeO_4 tetrahedra. Between these sheets there are two distinct cation sites that are occupied by the cations A, B and B'; the 2b site is coordinated by eight oxide ions at the vertices of a square antiprism and the 4f site by six at the vertices of an elongated, pseudo-tetragonal octahedron, see Fig. 1. The distribution of the cations over the two sites is determined by their relative size and charge. Our own research has focussed on compositions in which one or more of the cations is magnetic and we have previously reported the occurrence of paramagnetism, spin-glass behaviour, antiferromagnetism and weak ferromagnetism within the structure type [3–8]. Paramagnetism is likely to result when only one site is occupied by a magnetic cation, as in $Y_2CoGe_4O_{12}$ [3], but the behaviour of the more magnetically-concentrated compositions is difficult to predict because several inter-cation interactions are in competition with each other. In one report [8] we discussed compounds in which B' = Co and at least one of A and B was a magnetic cation from the f-block. In this case those compounds that underwent a magnetic transition did so at a temperature below 4 K and the interpretation of our data was consequently complicated by the interplay of crystal-field effects and spin-orbit coupling. More recently [9] we have described the behaviour of the magnetically-concentrated composition $ErFeCuGe_4O_{12}$ which orders antiferromagnetically at 20 K and undergoes a metamagnetic transition, driven by the single-ion anisotropy of Er^{3+}, in a field of 20 kOe at 2 K. Similar transitions have been seen in compositions with anisotropic Co^{2+} cations on the 4f sites [6]. In order to eliminate the consequences of orbital angular momentum and spin-orbit coupling we have begun to prepare compounds containing only spherical magnetic cations. We present below a discussion of $Gd_2CaGe_4O_{12}$ and $GdFeZnGe_4O_{12}$, each of which contains two isotropic magnetic cations with L = 0. In the former, both the magnetic cations are from the f-block, whereas the latter is a mixed f/d system. Our attempts to extend the study to include a compound containing three isotropic cations were thwarted when our attempts to prepare $GdMnFeGe_4O_{12}$ proved unsuccessful. The products of our two successful syntheses have been studied by magnetometry, Mössbauer spectroscopy and, in one case, neutron diffraction.

2. Experimental

Polycrystalline samples of $Gd_2CaGe_4O_{12}$ and $GdFeZnGe_4O_{12}$ were synthesised in solid-state reactions. The appropriate stoichiometric quantities of dried Gd_2O_3, $CaCO_3$, Fe_2O_3, ZnO, and GeO_2 were mixed thoroughly in an agate mortar, along with a 10% excess of GeO_2 to counteract its loss at high temperature [10]. The mixtures were heated at 1075 °C for 2 days with intermediate cooling and regrinding every day. They were then pressed into pellets and annealed at the same temperature for another 4 days with intermediate cooling and regrind-

* Corresponding author.
E-mail address: peter.battle@chem.ox.ac.uk (P.D. Battle).

https://doi.org/10.1016/j.jssc.2018.11.022
Received 10 October 2018; Received in revised form 13 November 2018; Accepted 14 November 2018
Available online 16 November 2018

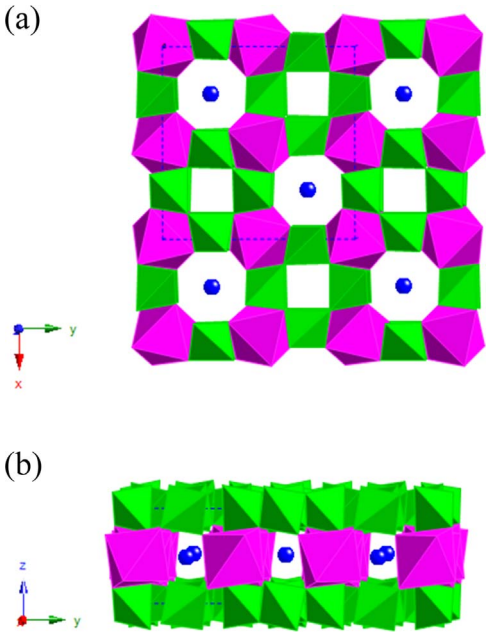

Fig. 1. Polyhedral representation of the crystal structure of $ABB'Ge_4O_{12}$ viewed along (a) [001] and (b) [100]: green tetrahedra and purple octahedra represent GeO_4 and $(B/B')O_6$ groups, respectively; blue circles represent *A* cations. (For interpretation of the references to color in this figure legend, the reader is referred to the web version of this article).

ing every two days. X-ray powder diffraction (XRPD) patterns were then collected at room temperature on a Panalytical Empyrean diffractometer using Cu $K\alpha_1$ radiation in order to assess the progress of the syntheses. Further heating at 1100 °C for 1 day was carried out if GeO_2 was detected in the product.

Magnetic measurements were performed using a Quantum Design MPMS XL SQUID magnetometer. DC susceptibility measurements were made while warming through the temperature range $2\ K \le T \le 300\ K$ in an applied field of 100 Oe after both zero-field cooling (ZFC) and field-cooling (FC) of the sample. The field dependence of the magnetization was measured over the range $-50 \le H/kOe \le 50$ at 2 K after the sample had been cooled in a magnetic field of 50 kOe. In the case of $GdFeZnGe_4O_{12}$ the field dependence of the magnetization was also measured at 10 K and the ac susceptibility was measured at frequencies of 1, 10 and 100 Hz over the temperature range $2 \le T/K \le 10$ in a 3.5 Oe ac drive field.

Mössbauer spectra were collected at temperatures selected in the light of the magnetometry data. ^{155}Gd spectra were collected at 5 K on both samples and at 20 K (above T_N) for $GdFeZnGe_4O_{12}$. The 50 mCi ^{155}Sm source and sample were mounted vertically in a helium flow cryostat and the Mössbauer drive was operated in sinusoidal mode. The 86.55 keV Mössbauer γ-photons were isolated from the various x-rays emitted by the source with a high-purity Ge detector. The system was calibrated using a laser interferometer with velocities crosschecked against ^{57}CoRh/α-Fe at room temperature and both $^{155}SmPd_3$/$GdFe_2$ and cubic Gd_2O_3 at 5 K. ^{57}Fe Mössbauer spectra were collected from polycrystalline samples of $GdFeZnGe_4O_{12}$ in the temperature range 5–20 K using a standard transmission spectrometer operated in sinusoidal mode with a ^{57}CoRh source. The drive velocity of the spectrometer was calibrated using a 6 μm thick α-Fe foil, at 295 K, and the isomer shift (δ) is quoted relative to the centre of the α-Fe calibration spectrum. The sample was held in a helium exchange gas and cooled using a vibration-isolated closed-cycle referigerator. All of the spectra were fitted using a non-linear least-square minimization routine derived from an exact solution to the full Hamiltonian [11].

Neutron powder diffraction (NPD) data were collected on $GdFeZnGe_4O_{12}$ using the 800-wire C2 powder diffractometer at the Canadian Neutron Beam Centre (CNBC), Chalk River, Ontario. The complex scattering length of gadolinium is dominated by an imaginary absorption term arising from nuclear resonances. The resulting energy dependence of the scattering length has been documented by Lynn and Seeger [12]. A large-area, flat-plate geometry was employed to reduce the impact of the very large neutron absorption cross section [13]. A closed-cycle refrigerator with the sample held in a helium exchange gas was used to cool the samples. Data were taken at two wavelengths. The primary experiments were conducted at a wavelength of 1.32806(6) Å (~1.33 Å). Patterns for full analysis were obtained at 3.6 K (40 h) and 20 K (30 h), well below and above T_N respectively. Additional, short-count patterns were obtained between these temperatures to track peak intensities and determine the magnetic ordering temperature. Finally, a 10-h pattern was obtained at 3.6 K with λ = 2.36963(8) Å (~2.37 Å). All refinements of the neutron diffraction patterns employed the FullProf/WinPlotr package [14,15]. Although data were collected over the full angular range of $3° \le 2\theta \le 83°$ allowed by the detector, the patterns were truncated for analysis at 2θ = 65° to minimise the effects of increasing absorption at larger scattering angles.

3. Results

X-ray powder diffraction indicated that the reaction products were essentially monophasic; a trace of $CaGeO_3$ could be seen in the pattern of $Gd_2CaGe_4O_{12}$, see Fig. S1. The iron-containing compound was brown and the calcium-containing composition was white. The diffraction patterns could both be indexed in the tetragonal space group *P*4/*nbm*; the structural parameters and cation distributions derived from these data are listed in Table 1.

The temperature dependence of the molar magnetic susceptibility of $Gd_2CaGe_4O_{12}$ is shown in Fig. 2. There is no evidence of a magnetic phase transition in the temperature range $2 \le T/K \le 300$ and the data can be accounted for by the Curie-Weiss Law with θ = -3.62(2) K and C = 15.463(1) $cm^3\ K\ mol^{-1}$, the latter corresponding to $\mu_{eff} = 7.84\ \mu_B$ per Gd^{3+} cation. The ^{155}Gd Mössbauer spectrum of $Gd_2CaGe_4O_{12}$ recorded at 5 K and shown in Fig. 3 consists of two well-resolved quadrupole doublets with relative areas of ~60% (inner doublet) and ~40% (outer doublet) these two components have been previously identified as being due to gadolinium in the 2*b* and 4*f* sites respectively [8]. The departure from the 50:50 area ratio demanded both by the stoichiometry and by the analysis of the x-ray diffraction pattern that shows that the 2*b* site is fully occupied by Gd and that the 4*f* site is occupied by an even mixture of Gd and Ca, is the result of weaker binding of Gd in the 4*f* site leading to a reduced recoil-free fraction and thus an underrepresentation of this component in the ^{155}Gd Mössbauer spectrum [8]. The fitted parameters are given in Table 2.

Table 1
Structural parameters of $Gd_2CaGe_4O_{12}$ and $GdFeZnGe_4O_{12}$ derived from XRPD.

		$Gd_2CaGe_4O_{12}$	$GdFeZnGe_4O_{12}$
a/Å		10.0766 (1)	9.7298(1)
c/Å		5.1043(1)	4.7515(1)
V/Å^3		518.28(1)	449.83(2)
Ge	*x*	0.5237(2)	0.5264(4)
O1	*x*	− 0.3673(9)	− 0.365(2)
	z	0.147(2)	0.178(3)
O2	*x*	0.1722(9)	0.154(2)
	y	0.0575(8)	0.054(1)
	z	0.257(2)	0.259(3)
2*b* occupancy		100% Gd	100% Gd
4*f* occupancy		50% Gd, 50% Ca	50% Fe, 50% Zn
R_{wp} %		7.33	10.05
χ^2		1.4	1.8

Space group *P*4/*nbm* (No. 125), Z = 2.
2*b* at (¼, ¼, ½); 4*f* at (0, 0, ½); Ge on 8*k* (*x*, ¼, 0); O1 on 8*m* (*x*, -*x*, *z*); O2 on 16*n* (*x*, *y*, *z*).
The constraint $U_{iso} = 0$ was used in both refinements.

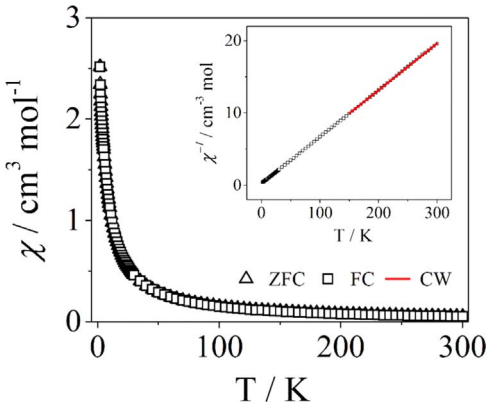

Fig. 2. Temperature dependence of the molar magnetic susceptibility and (inset) the inverse susceptibility of $Gd_2CaGe_4O_{12}$; Curie-Weiss parameters were obtained by fitting to the red points. (For interpretation of the references to color in this figure legend, the reader is referred to the web version of this article).

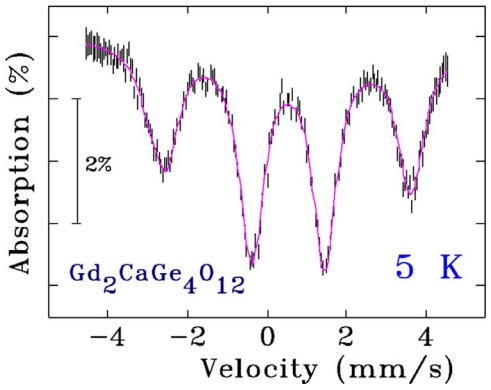

Fig. 3. ^{155}Gd Mössbauer spectrum of $Gd_2CaGe_4O_{12}$ recorded at 5 K showing the two distinct quadrupole doublets arising from Gd in the 2*b* (inner doublet) and 4*f* (outer doublet) sites respectively. The solid line is a fit described in the text.

Table 2
Fitted ^{155}Gd Mössbauer parameters for $Gd_2CaGe_4O_{12}$ at 5 K.

Site	IS mm/s	QS mm/s	Fraction %
2*b*	0.536(4)	3.88(2)	60(1)
4*f*	0.492(6)	13.24(2)	40(1)

The temperature dependence of the both the dc and ac susceptibilities of $GdFeZnGe_4O_{12}$ are shown in Fig. 4. The following parameters were derived by fitting the high-temperature dc data to the Curie-Weiss Law; $\theta = 7.37(2)$ K and $C = 12.198(1)$ cm^3 K mol^{-1}, the latter corresponding to $\mu_{eff} = 6.01\ \mu_B$ per Fe^{3+} ion when the moment of the Gd^{3+} cation is assumed to be $7.84\ \mu_B$. There is evidence for a magnetic transition at 13.2(2) K in both the dc and the ac data, although there is no clear maximum in $\chi(T)$ in either case. No significant imaginary component was detected in the ac susceptibility and data collected at three frequencies all overlie. $M(H)$ measured at 2 and 10 K is also shown in Fig. 4; both curves are non-linear and when H = 50 kOe the magnetization per formula unit takes a value of ~8 μ_B per mole at both temperatures. No hysteresis is present, nor is there any evidence for a metamagnetic transition.

^{155}Gd Mössbauer spectra of $GdFeZnGe_4O_{12}$ recorded at 20 and 5 K are shown in Fig. 5; the fitted parameters are listed in Table 3. At 20 K (well above T_N) the spectrum consists of a single quadrupole doublet as the 4*f* site is now fully occupied by a 50:50 Fe/Zn mixture and the Gd occurs only on the 2*b* site. Cooling to 5 K leads to the development of a magnetic hyperfine field as the moments order and the resulting spectrum is well fitted using a single, unbroadened, magnetic component. The simple form of the 5 K spectrum allows us to rule out complex incommensurate or modulated magnetic structures, all of which would lead to either multiple components or severely broadened lines.

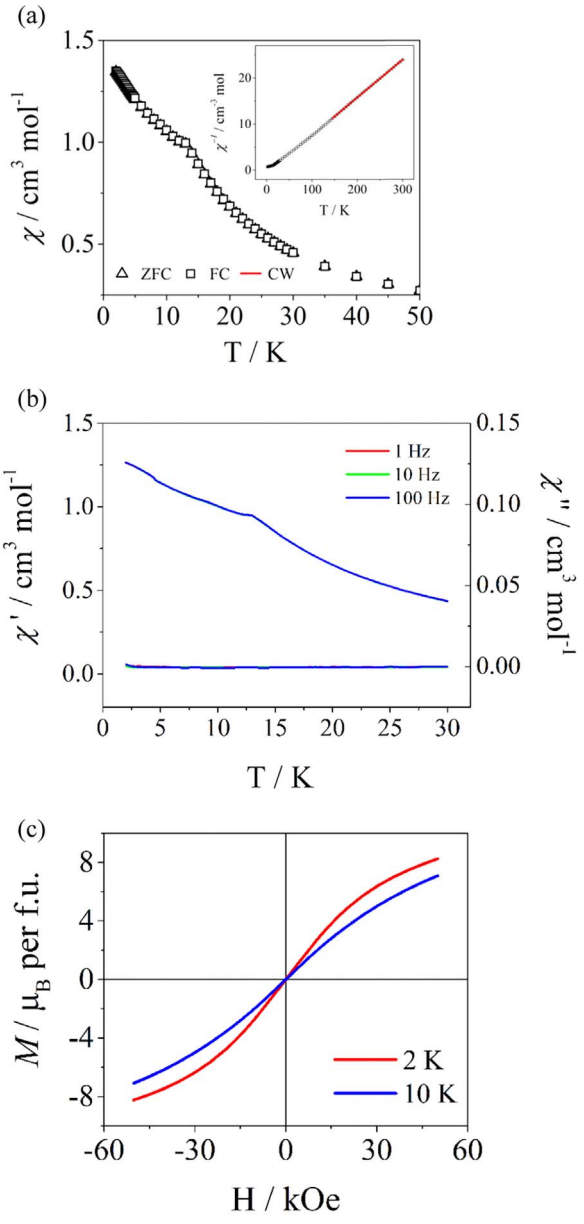

Fig. 4. (a) Temperature dependence of the molar magnetic susceptibility and (inset) the inverse susceptibility of $GdFeZnGe_4O_{12}$; Curie-Weiss parameters were obtained by fitting to the red points; (b) temperature dependence of the ac susceptibility of $GdFeZnGe_4O_{12}$ and (c) $M(H)$ of $GdFeZnGe_4O_{12}$ at 2 and 10 K. (For interpretation of the references to color in this figure legend, the reader is referred to the web version of this article).

The series of ^{57}Fe Mössbauer spectra for $GdFeZnGe_4O_{12}$ shown in Fig. 6 confirm the iron in this system also orders magnetically. The spectrum at 15 K could be interpreted as being from an Fe^{2+} system with an unusually low isomer shift or from an Fe^{3+} system with an unusually large quadrupole splitting (QS). The inflexibility of the oxidation states of the other elements in the compound, together with the colour of the sample and value of the effective magnetic moment derived from our susceptibility data, strongly suggests that Fe^{3+} is present. The large QS can be attributed to the low, 2/*m*, point symmetry at the 4*f* site and the resulting irregularity of the FeO_6 coordination polyhedron. We encountered a similar situation in our study of $YFeMnGe_4O_{12}$ [5]. We note that a minor (~5%) ferric impurity is evident near the centre of the spectrum. At 5 K the spectrum shows

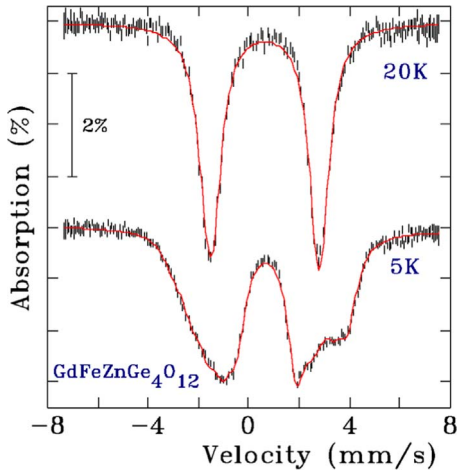

Fig. 5. ^{155}Gd Mössbauer spectra of $GdFeZnGe_4O_{12}$ recorded at 20 K and 5 K. The paramagnetic pattern at 20 K shows a single quadrupole doublet associated with Gd in the 2*b* site, while the magnetic pattern obtained at 5 K reflects a single well-defined magnetic environment for the Gd. The solid lines are fits described in the text.

Table 3
Fitted ^{155}Gd Mössbauer parameters for $GdFeZnGe_4O_{12}$.

TK	IS mm/s	QS mm/s	B_{hf} T	θ degrees
20	0.634(4)	9.159(2)		
5	0.674(5)	9.159(-)	25.1(1)	74(1)

Note: QS at 5 K was not fitted, it was constrained to the 20 K value. θ is the angle between B_{hf} and V_{ZZ}.

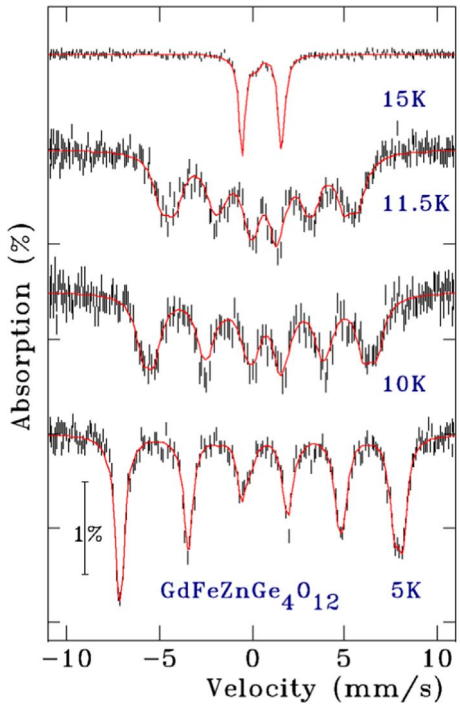

Fig. 6. ^{57}Fe Mössbauer spectra of $GdFeZnGe_4O_{12}$ recorded between 5 K and 15 K showing the evolution of the magnetic order. The paramagnetic pattern at 15 K shows a single quadrupole doublet associated with ferric iron in the 4*f* site. At 5 K the magnetic sextet is clearly asymmetric reflecting a more complex magnetic environment for the iron. See text for details. In the 15 K spectrum there is a small ferric impurity apparent as a shoulder at about 0 mm/s.

the well-split magnetic sextet expected for a magnetically ordered Fe^{3+} system. However, the spectrum is clearly asymmetric (the leftmost line is deeper and sharper than the rightmost line) indicating that, unlike

Table 4
Fitted ^{57}Fe Mössbauer parameters for $GdFeZnGe_4O_{12}$.

TK	IS mm/s	QS mm/s	B_{hf} T	θ degrees
15	0.545(3)	2.136(5)		
5	0.549(7)	2.136(-)	44.8(1)	69(1)
5	0.549(7)	2.136(-)	45.6(1)	56(1)

Note: The isomer shifts at 5 K were constrained to be equal for the two components as they arise from a magnetic environment change, and not a change in the chemical environment. The QS value was constrained to that found at 15 K.

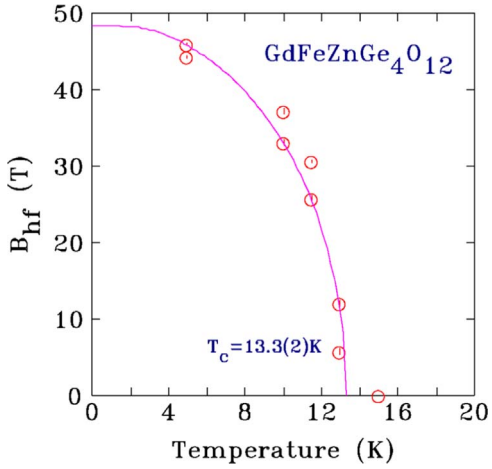

Fig. 7. Temperature dependence of the ^{57}Fe hyperfine field (B_{hf}) in $GdFeZnGe_4O_{12}$. The solid line is a fit to a $J = 5/2$ Brillouin function giving an ordering temperature of 13.3(2) K. The two points at each temperature are derived from the two-site fit; this is likely to be a simplification of the actual, more complex, distribution of iron environments.

the gadolinium, the iron does not experience a single magnetic environment. The simplest decomposition that yielded a good fit was to use two equal area components with very slightly different hyperfine fields and slightly different angles between the local hyperfine field and the principal axis of the electric field gradient tensor (V_{zz}). This is the fit shown in Fig. 6 and the fitted parameters are listed in Table 4. However, the Fe^{3+} cations in this compound all occupy the same crystallographic site and the spectral broadening is therefore more likely to stem from the presence of a range of fields than from a well-defined two-site scenario, with the range of fields being a consequence of the range of environments created by the disordered distribution of Zn^{2+} and Fe^{3+} cations. In that case the two distinct sites described in Table 4 do not actually exist, but the difference between the two values of B_{hf} gives an indication of the range of fields present. No paramagnetic spins are present at 5 K. We shall return to this point below. Tracking the evolution of B_{hf} with temperature and fitting it to a $J = 5/2$ Brillouin function yields an ordering temperature of 13.3(2) K (Fig. 7).

Powder neutron diffraction patterns for $GdFeZnGe_4O_{12}$ taken at 20 K and 3.6 K using a wavelength of ~1.33 Å are shown in Fig. 8 along with a difference pattern constructed by subtracting the 20 K pattern from the 3.6 K pattern to yield the magnetic-only scattering signal. It is immediately clear that several new peaks appear as the material orders magnetically. Tracking the intensity of two of these peaks as a function of temperature (Fig. 9) yields an ordering temperature of 13.8(2) K, fully consistent with that derived above from the ^{57}Fe Mössbauer spectra. The lowest angle magnetic peak near 2θ ~8° could be indexed as (00½), suggesting a simple commensurate magnetic structure that is doubled along the c-axis. A search for lower-*q* peaks that could reflect a longer period modulation of the structure was carried out by collecting a pattern using λ~2.37 Å. No new peaks were detected. In order to determine the symmetry-allowed magnetic structures for the Gd and Fe sites in the *P*4/*nbm* nuclear space group with a propagation

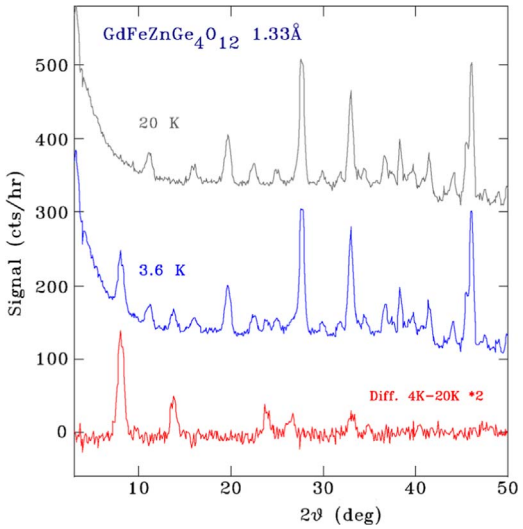

Fig. 8. Powder neutron diffraction patterns of $GdFeZnGe_4O_{12}$ taken at 20 K (top) and 3.6 K (middle) at a wavelength of ~1.33 Å. The bottom curve is a magnetic-only scattering pattern generated by subtracting the 20 K pattern from the 3.6 K pattern to remove the nuclear contributions.

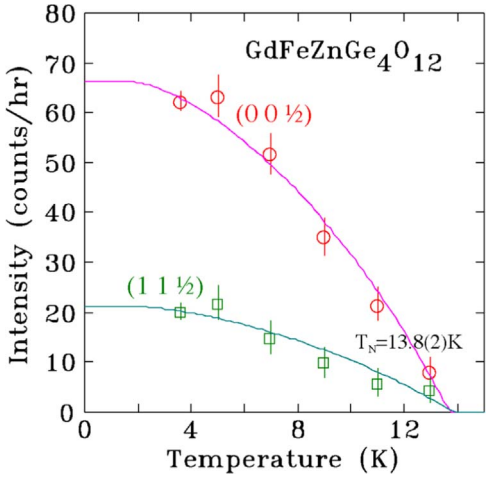

Fig. 9. Temperature dependence of the intensity of the two strongest magnetic peaks seen in Fig. 8 (the (00½) peak at 2θ ~8° and the (11½) peak seen at 2θ ~13°). Fits to $J = 5/2$ Brillouin functions (squared because the intensity scales as moment-squared) yields an ordering temperature of 13.8(2) K.

vector k = [0 0 ½], we carried out Representational Analysis using the BASIREPS program [15]. A simple planar antiferromagnetic (AF) structure with all of the Gd and Fe moments parallel to each other within the *ab*-plane and coupled AF along the *c*-axis, i.e. an A-type AF [16], was found to give the best fit to the observed diffraction pattern. During this analysis the atomic coordinates were held at the values determined by XRPD and all the displacement parameters were set to zero. The magnetic structure can be described in the magnetic space group $P_{2c}b'an$ (No. 50.9.385) [17]. The fit to the observed patterns (shown in the upper panel of Fig. 10) gave moments of 5.5(3) μ_B and 4.2(4) μ_B for Gd and Fe respectively, while the agreement factors were $R_{wpr} = 4.1\%$ and $\chi^2 = 10.1$. It is apparent from Fig. 10 that two large regions were formally excluded due to interference from the sample mount and that there are other areas of minor contamination which could be affecting the reliability of the fit. The rapidly-rising background under the broad magnetic peak at ~8° also caused problems in the fitting process. In order to confirm that the derived magnetic structure is indeed correct, a magnetic-only scattering pattern was therefore generated by subtracting the 20 K pattern from the 3.6 K pattern (appropriately scaled for the different counting times) and

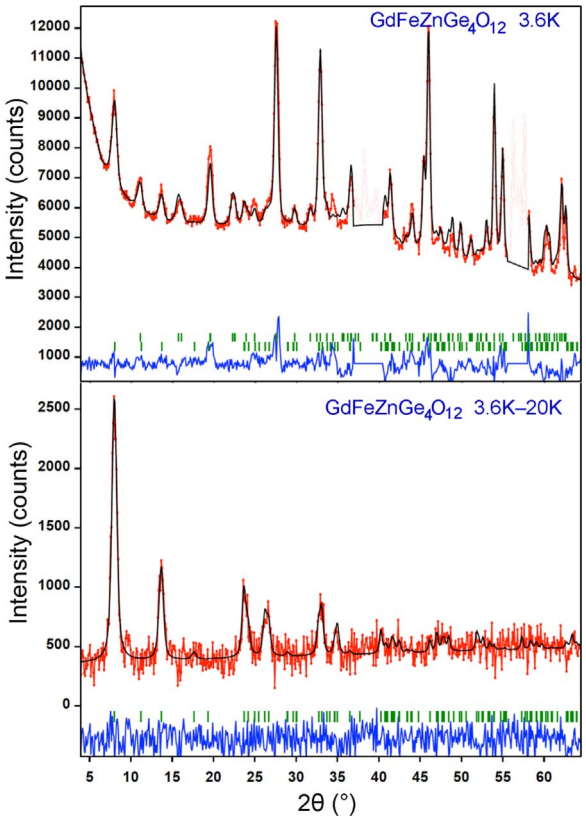

Fig. 10. Top panel: FullProf fit to the powder neutron diffraction pattern of $GdFeZnGe_4O_{12}$ taken at 3.6 K. The Bragg markers are for (top) nuclear and (bottom) magnetic contributions. Two regions near 2θ ~38° and 2θ ~55° were excluded due to interference from the sample mount. Bottom panel: FullProf fit to the magnetic-only difference pattern (offset by +500 counts) showing that all of the magnetic features are correctly fitted by the identified magnetic structure.

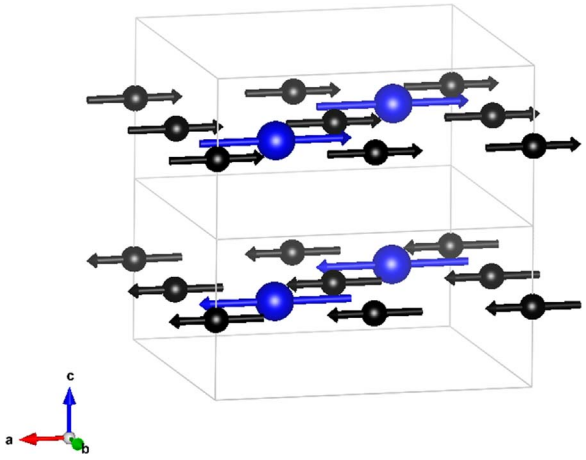

Fig. 11. Derived magnetic structure for $GdFeZnGe_4O_{12}$ showing the alternating ferromagnetic *ab*-planes of Gd (blue) and Fe (black) moments that are coupled AF along the *c*-axis. The non-magnetic ions (Zn, Ge and O) have been omitted for clarity. (For interpretation of the references to color in this figure legend, the reader is referred to the web version of this article).

fitted with the lattice parameters and scale factor constrained to those from the direct fit to the 3.6 K pattern. This procedure, which involved the refinement of only the instrument zero-point, two background parameters and two atomic moments, eliminates correlations between the nuclear and magnetic models. The resulting fit, shown in the lower panel of Fig. 10, clearly shows that all of the magnetic peaks are accounted for both in position and intensity; the calculated pattern does not include any features that do not appear in the data, nor are

there features in the data that are not fitted. We therefore conclude that the magnetic structure illustrated in Fig. 11 is correct. The ordered atomic moments derived in this way were 6.02(13) and 3.84(15) μ_B for Gd^{3+} and Fe^{3+}, respectively. These more precise values will form the basis of the discussion that follows.

4. Discussion

We cannot enter into a detailed analysis of the crystal structures of $Gd_2CaGe_4O_{12}$ and $GdFeZnGe_4O_{12}$ because the atomic coordinates derived from our XRPD data, see Table 1, lack the necessary precision, particularly in the case of the lightest atoms, O1 and O2. However, our results do show that the $GdBB'Ge_4O_{12}$ framework is able to accommodate both GdCa and FeZn as BB' pairings on the 4*f* sites, even though these pairs have very different mean ionic radii [18] of 0.97 and 0.69 Å, respectively. In order to achieve this, the unit cell volume changes by ~15%, with the unit cell parameters *a* and *c* changing by 3.6% and 7.4%, respectively. Thus, given that $a \sim 2c$, the pseudo-cubic character of the 4*f* sublattice is maintained as the composition changes.

Our Mössbauer and magnetometry data show that $Gd_2CaGe_4O_{12}$ is paramagnetic throughout the measured temperature range. The magnetic interactions between the *f*-block cations on the 2*b* sites and 50% of the 4*f* sites are too weak to lead to the onset of magnetic ordering. In contrast, our NPD data show that the *f*-block cations and the *d*-block cations in $GdFeZnGe_4O_{12}$ are antiferromagnetically ordered below 13.8(2) K. The transition is also apparent in the Mössbauer spectra and in χ(T), although the latter retains a negative gradient below T_N; this residual paramagnetism might be attributable to the impurity phase that was detected by Mössbauer spectroscopy but not by diffraction methods. The transition temperature is higher than those of ~4 K reported previously for $Gd_2CoGe_4O_{12}$, $GdScCoGe_4O_{12}$ and $GdLuCoGe_4O_{12}$ [8] and it approaches, but remains below, the transition temperatures, $15 \le T/K \le 17$, observed in AMnFeGe$_4$O$_{12}$ (A = Y, Eu, Lu). It is also lower than that of the more magnetically-concentrated composition $ErFeCuGe_4O_{12}$ [9]. The magnetic superexchange pathways that might be important in this crystal structure have been described in detail elsewhere [4]. We assume that the superexchange between *d*-block cations along Fe–O–Ge–O–Fe pathways is the dominant interaction in these compounds and that the moments of the *f*-block cations on the 2*b* sites are aligned by the internal field created at the 4*f* sites. The behaviour of $M(H)$, which reaches a value greater than 7 μ_B in a field of 50 kOe, supports the idea that the Gd^{3+} cations are only weakly coupled into the AF structure (see Fig. 4). Hence we attribute the reduction in the Néel temperature of $GdFeZnGe_4O_{12}$, relative to those of AMnFeGe$_4$O$_{12}$, to the 50% dilution of the pseudo-cubic 4*f* sublattice by diamagnetic Zn^{2+}. The AMnFeGe$_4$O$_{12}$ compositions adopt an A-type structure with the atomic moments aligning in ferromagnetic sheets perpendicular to [001] and $GdFeZnGe_4O_{12}$ does likewise, with the Gd^{3+} moments aligning parallel to the moments of the Fe^{3+} cations in the same ferromagnetic *xy* sheet. We note that the anisotropy of Er^{3+} dictates that the moments in $ErFeCuGe_4O_{12}$ align along [001]. The adoption of an A-type structure suggests that the interactions between next-nearest-neighbour cations are stronger than those between nearest neighbours. We have previously proposed [5] that the relative size of the cations on the 2*b* and 4*f* sites determines the type of ordering adopted because it determines the tilt angle of the octahedra of oxide ions that surrounds the 4*f* site, and hence the bond angles along the superexchange pathway. In the case of $GdFeZnGe_4O_{12}$ the low value, 0.658, of the ratio $\langle r_{4f} \rangle / r_{2b}$ would be expected to lead to the observed $\mathbf{k} = [0, 0, ½]$ magnetic structure. It is not clear why the ordering temperature of $GdFeZnGe_4O_{12}$ is higher, by a factor of three, than those of $Gd_2CoGe_4O_{12}$, $GdScCoGe_4O_{12}$ and $GdLuCoGe_4O_{12}$ [8]. It could also be argued that, if the magnetic ordering is controlled only by the *d*-block cations, then $Y_2CoGe_4O_{12}$ [3] is as likely to order as $GdFeZnGe_4O_{12}$ because they both have magnetic cations on 50% of the 4*f* sites. We suggest that the higher moment of $S = 5/2$ Fe^{3+} is likely to be a crucial factor, as are the lower ionic radius and higher charge which will lead to shorter and stronger Fe–O–Ge–O–Fe superexchange pathways. Finally we note that 13.8 K is a relatively high ordering temperature for Gd^{3+} cations; although the Fe^{3+} sublattice in the perovskite $GdFeO_3$ orders at ~660 K [19], the Gd^{3+} cations only order at 2.2 K [20].

The fitted ^{155}Gd Mössbauer parameters listed in Table 3 are typical of Gd^{3+} compounds [21]. The unusually large Fe^{3+} QS observed in the ^{57}Fe spectra has been discussed above, as has the need to use a distribution of fields to fit the spectrum collected at 5 K. These fields are lower than the values measured in other compounds having superexchange pathways of comparable complexity, as is the ordered moment measured by neutron diffraction [22,23]. The presence of line broadening in the low-temperature Mössbauer spectrum and the relatively low value of the ordered moment are reminiscent of the perovskite $SrLaFeSnO_6$ [24,25]. That compound has a disordered distribution of Fe^{3+} and diamagnetic Sn^{4+} cations over the sites on a simple cubic lattice. It orders as a G-type antiferromagnet below 38 K with an ordered moment of only 2.94(4) μ_B per Fe^{3+} cation at 1.7 K. Thus, although the superexchange pathways are clearly very different, there are similarities between $SrLaFeSnO_6$ and $GdFeZnGe_4O_{12}$. In the case of $SrLaFeSnO_6$ the low value of the ordered moment was explained by postulating that not all of the cations are part of the long-range magnetic ordering that percolates through the structure, but that, as a consequence of the disruption of the magnetic connectivity caused by the Fe/Sn disorder, some of them are part of magnetically-ordered clusters of varying size that are not coupled to the percolating structure. They consequently do not contribute to the magnetic Bragg scattering but they do appear as static, rather than paramagnetic, spins in the Mössbauer spectrum. It is possible that similar spin disorder exists in $GdFeZnGe_4O_{12}$. In that case the observed broadening of the spectral lines would not be directly due to variations in the local structure caused by Fe/Zn disorder, but to the magnetic disorder introduced by the presence of the clusters. Their presence also offers an alternative explanation for the continued increase of the magnetic susceptibility of $GdFeZnGe_4O_{12}$ when the sample is cooled below T_N. Further experimental work will be necessary before this hypothesis can be confirmed. We note that the ordered moment of the Gd^{3+} cations on the 2*b* sublattice is also reduced below the expected value, $gS = 7$ μ_B. We suggest that the missing spins are in the regions that are relatively rich in zinc, and therefore do not couple to the percolating structure.

5. Conclusions

$Gd_2CaGe_4O_{12}$ and $GdFeZnGe_4O_{12}$ are isostructural with $SrNa_2P_4O_{12}$. The calcium-containing composition is paramagnetic above 2 K whereas $GdFeZnGe_4O_{12}$ is antiferromagnetic below 13.8 K(2) K. It is proposed that the observation of magnetic order at what is, for this structure type, a relatively high temperature, can be attributed to the small size, high charge and high spin of the Fe^{3+} cations. The structural disorder, that is the random distribution of Fe^{3+} and Zn^{2+} cations over the 4*f* sites, results in a relatively low value for the ordered moment of both Gd^{3+} and Fe^{3+} in the antiferromagnetic phase.

Acknowledgments

DHR gratefully acknowledges useful discussions with J.M. Cadogan (UNSW-Canberra) and experimental assistance from C. D. Boyer at CNBC. Financial support for this work was provided by the Natural Sciences and Engineering Research Council of Canada and the Fonds Quebecois de la Recherche sur la Nature et les Technologies.

Appendix A. Supplementary material

Supplementary data associated with this article can be found in the online version at doi:10.1016/j.jssc.2018.11.022.

References

[1] I.I. Leonidov, V.G. Zubkov, A.P. Tyutyunnik, N.V. Tarakina, L.L. Surat, O.V. Koryakova, E.G. Vovkotrub, J. Alloy. Compd. 509 (2011) 1339–1346.
[2] M.T. Averbuch-Pouchot, A. Durif, Acta Crystallogr. Sect. C. Cryst. Struct. Commun. 39 (1983) 811–812.
[3] X.-Q. Liu, P.D. Battle, J. Ridout, D. Xu, S. Ramos, J. Solid State Chem. 228 (2015) 183–188.
[4] D. Xu, M. Avdeev, P.D. Battle, J. Solid State Chem. 265 (2018) 339–344.
[5] D. Xu, M. Avdeev, P.D. Battle, J.M. Cadogan, H. Lamont, J. Solid State Chem. 254 (2017) 40–46.
[6] D. Xu, M. Avdeev, P.D. Battle, X.Q. Liu, Inorg. Chem. 56 (2017) 2750–2762.
[7] D. Xu, M. Sale, M. Avdeev, C.D. Ling, P.D. Battle, Dalton Trans. 46 (2017) 6921–6933.
[8] D.M. Xu, M. Avdeev, P.D. Battle, D.H. Ryan, Dalton Trans. 46 (2017) 15778–15788.
[9] D. Xu, M. Avdeev, P.D. Battle, J. Solid State Chem. 269 (2019) 107–112.
[10] C. Taviot-Gueho, P. Leone, P. Palvadeau, J. Rouxel, J. Solid State Chem. 143 (1999) 145–150.
[11] C.J. Voyer, D.H. Ryan, Hyperfine Interact. 170 (2006) 91–104.
[12] J.E. Lynn, P.A. Seeger, At. Data Nucl. Data Tables 44 (1990) 191–207.
[13] D.H. Ryan, L.M.D. Cranswick, J. Appl. Crystallogr. 41 (2008) 198–205.
[14] T. Roisnel, J. Rodriguez-Carvajal, Mater. Sci. Forum 378–381 (2001) 118–123.
[15] J. Rodriguez-Carvajal, Phys. B Condens. Matter 192 (1993) 55–69.
[16] E.O. Wollan, W.C. Koehler, Phys. Rev. 100 (1955) 545–563.
[17] J.M. Perez-Mato, S.V. Gallego, E.S. Tasci, L. Elcoro, G. de la Flor, M.I. Aroyo, Ann. Rev. Mater. Res. 45 (2015) 217–248.
[18] R.D. Shannon, Acta Crystallogr. A 32 (1976) 751.
[19] D. Treves, J. Appl. Phys. 36 (1965) 1033–1039.
[20] F.B. Zhang, S.J. Li, J.D. Song, J. Shi, X.F. Sun, IEEE Trans. Magn. 51 (2015).
[21] G. Czjzek, G.J. Long, F. Grandjean (Eds.), Mossbauer Spectroscopy Applied to Magnetism and Materials Science, Plenum Press, New York, 1993, pp. 373–429.
[22] P.D. Battle, A.K. Cheetham, G.J. Long, G. Longworth, Inorg. Chem. 21 (1982) 4223–4228.
[23] G.J. Long, G. Longworth, P. Battle, A.K. Cheetham, R.V. Thundathil, D. Beveridge, Inorg. Chem. 18 (1979) 624–632.
[24] M.P. Attfield, P.D. Battle, S.K. Bollen, T.C. Gibb, R.J. Whitehead, J. Solid State Chem. 100 (1992) 37.
[25] T.C. Gibb, J. Mater. Chem. 2 (1992) 415.